Water Resources Research

RESEARCH ARTICLE
10.1029/2019WR026602

Idealized Model for the Deflection of Sediment Into Lateral Branches of Lowland Rivers

K. Kästner[1] and A. J. F. Hoitink[2]

[1]Asian School of the Environment, Nanyang Technological University, Singapore, [2]Hydrology and Quantitative Water Management Group, Wageningen University and Research, Wageningen, Netherlands

Key Points:

- Diversion of sediment into a lateral branch of a lowland river is strongly influenced by the local size and aspect ratio at the inlet
- The excess amount of diverted sediment decreases with the local cross-section area and depth at the inlet
- Local inlet morphodynamics likely influences the regional evolution of fluvial channel networks

Correspondence to:
A. J. F. Hoitink,
ton.hoitink@wur.nl

Citation:
Kästner, K., & Hoitink, A. J. F. (2020). Idealized model for the deflection of sediment into lateral branches of lowland rivers. *Water Resources Research*, *56*, e2019WR026602. https://doi.org/10.1029/2019WR026602

Received 24 OCT 2019
Accepted 29 APR 2020
Accepted article online 13 MAY 2020

This article was prematurely published without the authors' corrections. Corrections were made on 24 June 2020, to incorporate the author's changes.

Abstract The division of sediment at river bifurcations is crucial for the morphodynamics of anastamosing rivers and distributary delta channel networks. Many river bifurcations are strongly asymmetric and have a planform where a small channel branches off to the side. Such a configuration is also typical for man-made diversions of water and sediment into canals. At asymmetric bifurcations, the division of sediment is influenced by the secondary current, which is caused by the turning of the flow toward the side. The secondary currents cause especially water from the lower parts of the water column to be diverted into the side branch. As the sediment concentration close to the bottom is high, side branches can receive a disproportionately large fraction of the incoming sediment load, relative to the water discharge. Lateral diversions have been extensively studied with physical and numerical experiments, with the goal to either mitigate or exploit this effect. However, a systematic mathematical analysis of the parameter space has not yet appeared in the literature. Here, we present a comprehensive analysis by way of an idealized model, revealing how the division of sediment is influenced by the width and depth of the branches. We show that the excess of sediment that is diverted into the side branch is lower when the inlet to the side branch is wider and shallower. This may have larger implications for the stability of delta channel networks, as inlets to side branches tend to be locally wider, which likely contributes to their morphological stability.

1. Introduction

The division of sediment at river bifurcations is crucial for the evolution of fluvial channel networks. A network can be highly dynamic when the sediment that arrives at a bifurcation is not divided among the bifurcation branches in proportion to their transport capacity, as a branch that receives more sediment than what it can carry fills in, while a branch that receives less sediment scours and widens (Sloff et al., 2013; Wang et al., 1995). This can have dire consequences, as channels can become defunct or infrastructure become undermined (Bateman et al., 2009; Doets, 2015; Edmonds, 2012; Goodfriend & Stanley, 1999; Mendoza et al., 2016; Morozova, 2005).

Many river bifurcations are very asymmetric so that one of the branches receives a larger part of the discharge and is much wider than the other one. The asymmetry is often reflected in the planform of a bifurcation. The approaching channel and main branch nearly form a continuous reach, while the smaller channel branches off to the side. This configuration is similar to that of man-made lateral diversions. Such diversions have historically been studied in the laboratory by Bulle (1926), Habermaas (1935), Riad (1961), and Herrero et al. (2015), as well as recently with large-scale computer simulations by Shettar and Murthy (1996), Neary et al. (1999), Gaweesh and Meselhe (2016), and Dutta et al. (2017). The experiments show that in proportion to the discharge, a larger fraction of sediment is diverted into a side branch. This is because the turning of the flow into the side branch induces a secondary current, which primarily diverts water from the lower part of the water column, which carries most of the sediment, into the side branch. This is in contrast to what may be expected from the transport capacity of the branches, as the transport capacity decreases more rapidly than the size of a branch (Wang et al., 1995). This implies that side branches fill in over time.

Despite the experimental results, many asymmetric bifurcations in river deltas have been stable over extended periods, which suggests that the sediment is divided in proportion to the transport capacity of the branches. Thus, there seem to be factors that counteract the steering of sediment by the secondary flow. In gravel-bed rivers, bifurcations can be stabilized by a transverse slope across the approaching channel,

which directs bed material into the larger and deeper branch (Bolla Pittaluga et al., 2003, 2015; Redolfi et al., 2016). However, the transverse slope does not seem to be the factor that stabilizes deltaic bifurcations of large sand-bed rivers (Buschman et al., 2010; Kästner & Hoitink, 2019; Sassi et al., 2013). Large sand-bed rivers transport sediment predominantly in suspension, which can reduce the effect of the secondary flow and is known to affect the dynamics of avulsion channels (Slingerland & Smith, 1998). Another factor that can influence the division of sediment is the curvature of the upstream channel, as the secondary flow in meander bends can steer sediment toward branches located in the inner bend (Kleinhans et al., 2008) and as transverse material sorting can influence the division (Sloff & Mosselman, 2012). Another contributing factor is the migration of river banks. Channels in scale models typically have fixed banks and a regular geometry, so that they intersect with sharp corners. This entails different flow and sediment transport patterns than in natural channels, where the transition between channels is smooth. Flow separation is reduced or absent due to the absence of a sharp corner, and the larger effective width reduces the strength of the flow. Bank migration can also increase the bifurcation angle over time (De Heer & Mosselman, 2004; Kästner & Hoitink, 2019). Some scale experiments with different bifurcation angles and smoothed banklines have been conducted (Bulle, 1926; Riad, 1961), but so far, no model has been developed that incorporates these factors to simulate their evolution over time, as the bank migrates. Due to a lack of sufficient empirical evidence from the field, it remains uncertain which factors govern the division of sediment and hence determine the stability of bifurcations of large sand-bed rivers (Kleinhans et al., 2013). Likely, reasons differ from case to case.

Several empirical relations for the division of sediment into lateral branches have been proposed (Meijer & Ksiazek, 1994; Raudkivi, 1993; Van der Mark & Mosselman, 2013). These relations are curves fitted to physical and numerical experiments. However, until now, the parameter space has not been systematically analyzed, and no mathematical model has been brought forward that determines the division of sediment at a lateral diversion. Here, we take the first step toward a generic model that accounts for the influence of the secondary flow on the division of sediment at lateral diversions.

We base our model on the observation that the division of sediment is closely related to the streamlines of the near-bed flow (Raudkivi, 1993). While the division of water is determined to the dividing streamline of the depth-averaged flow, the division of bedload is linked to the streamline of the near-bed flow. Both the streamlines of the depth-averaged and near-bed flow curve toward the diversion, but the secondary flow causes the arc near the bed to be larger. Van der Mark and Mosselman (2013) considered this in their empirical model, albeit in a rather ad hoc manner. We circumvent the preclusion of a particular functional relationship, by directly determining the dividing streamline of the flow. This is made possible by the observation that the velocity at an idealized bifurcation closely resembles that of potential flow (Hager, 1984), which can be determined on hand of simple expressions. These also give insight into the influence of the parameters on the division of sediment.

Potential flow has been applied to determine the velocity at lateral diversions by Modi et al. (1981), Sinha and Odgaard (1996), Hassenpflug (1998), and Kacimov (2000). These studies focus on the computation of the depth-averaged flow, but none of those studies explored the near-bed flow nor its parameter space. Nevertheless, the near-bed flow and the sediment division can be readily approximated from the depth-averaged flow (Kawai et al., 1993; Raudkivi, 1993). Here, we determine the division of sediment at a lateral diversion with idealized geometry based on potential flow. We explore how the width and depth of the channels, as well as the division of discharge, influence the division of sediment. With the channel dimensions, we consider the most essential parameter set. Our model can serve as a basis to investigate more complex geometries with arbitrary bifurcation angle and inlet shape, bathymetry, or flow separation in the side branch.

2. Flow at a Lateral Diversion

The division of water can be understood on the hand of the streamlines of the depth-averaged flow. The flow near the right bank is diverted into the side branch, and the corresponding streamlines are turning into the side branch. There is one streamline, the dividing streamline, which separates the part of the flow that enters the side branch from that remaining in the main channel (figure 1). Similarly, the division of sediment can be understood on the hand of the streamlines of the near-bed flow, as the sediment is predominantly transported near the bed. The turning of the flow into the side branch induces a secondary flow orthogonal with respect to the streamline, which is directed inward near the bed and outward near the surface. As a

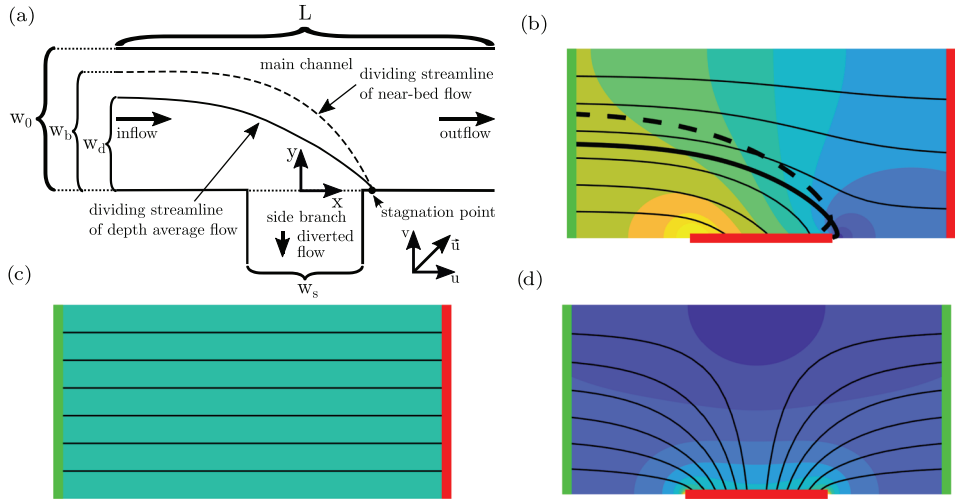

Figure 1. (a) Schema of the lateral diversion; (b) streamlines and magnitude of the flow, as the superposition of (c) the flow along the main branch; and (d) flow into the diversion, dividing streamline of the depth-averaged flow is bold, and that of the near-bed flow dashed; red boundaries indicate outflow and green boundaries inflow. Note that the side branch does not necessarily have to take off at an angle of 90°. Slanted side branches can be accounted for, by noticing that width of the inlet scales to the width of the side branch as $\frac{1}{\sin\theta}$, where θ is the angle between the main channel and side branch.

result, most water enters the side branch from the lower part of the water column. The secondary flow also results in a wider turn of the dividing streamline of the near-bed flow. Sediment transported as bedload is divided by the dividing streamline of the near-bed flow (Raudkivi, 1993). In the remaining part of the section, we determine the flow at a lateral diversion with idealized geometry and show how on hand of the streamlines the division of sediment can be determined.

2.1. Flow at a Lateral Diversion From a Wide Channel

We consider a highly idealized geometry, where the main channel has a rectangular cross section with constant width and a horizontal bed. The inlet to the side branch has also a rectangular cross section, with the same bed level as the main channel.

We assume that the flow is stationary and that the momentum balance is dominated by advective acceleration so that the depth-averaged flow is determined by continuity alone:

$$\Delta \cdot (\mathbf{h}\vec{\mathbf{u}}) = \frac{\partial \mathbf{hu}}{\partial \mathbf{x}} + \frac{\partial \mathbf{hv}}{\partial \mathbf{y}} = 0, \tag{1}$$

where $\mathbf{u}$ is the velocity component pointing in the direction of the main channel and $\mathbf{v}$ is the orthogonal velocity component pointing across the main branch toward the side branch. $\mathbf{x}$ and $\mathbf{y}$ are the corresponding coordinates, along and across the main branch, respectively, and $\mathbf{h}$ is the channel depth. Bold symbols stand for variables in natural dimensions, while the italic variables and operators introduced below are normalized to unit dimensions. We consider flow with a small Froude number and hence neglect the perturbation of the surface elevation by the flow.

Without loss of generality, we center the diversions at $\vec{x} = (x, y) = (0, 0)$ and denominate the length of the main channel as L. We only consider the case where the main channel is long, that is, $L \to \infty$. The boundary conditions for the case of uniform depth ($\Delta \mathbf{h} = 0$) are

$$\mathbf{u}\left(-\frac{1}{2}\mathbf{L}, \mathbf{y}\right) = \mathbf{u}_{\text{in}}, \mathbf{u}\left(+\frac{1}{2}\mathbf{L}, \mathbf{y}\right) = \mathbf{u}_{\text{in}} - \frac{\mathrm{w}_s}{\mathbf{w_0}}\mathbf{v}_0, \tag{2a}$$

$$\mathbf{v}(\mathbf{x}, -\mathbf{w_0}) = 0, \mathbf{v}(\mathbf{x}, 0) = \mathbf{v}_0\, \mathbf{f}, \tag{2b}$$

where $\mathbf{w_0}$ and w_s are the widths of the main channel and inlet to the side branch, respectively. $\mathbf{v}_0$ is velocity averaged across the inlet. The function $\mathbf{f}$ represents the velocity profile of the flow across the inlet and is

elsewhere on the right bank equal to zero. $\mathbf{Q}_{\text{in}} = \mathbf{u}_{\text{in}}\,\mathbf{h}\,\mathbf{w_0}$ and $\mathbf{Q}_{\text{s}} = \mathbf{v}_0\,\mathbf{h}\int_{-\frac{1}{2}\mathrm{w_s}}^{\frac{1}{2}\mathrm{w_s}} \mathbf{f}\mathrm{d}\mathbf{x} = \mathbf{v}_0\,\mathbf{h}\,\mathbf{w_0}$ are the discharges in the approaching channel and in the side branch, respectively. The system is conservative; that is, the inflow discharge is balanced by the sum of the two outflow discharges.

The velocity is uniquely determined by the univariate velocity potential Φ, with $\mathbf{u} = -\frac{\alpha\Phi}{\alpha\mathbf{x}}$, $\mathbf{v} = -\frac{\alpha\Phi}{\alpha\mathbf{y}}$ so that the continuity equation (1) simplifies to an equation in one variable:

$$\Delta\mathbf{h}\cdot\Delta\Phi + \mathbf{h}\,\Delta\Phi = 0, \tag{3}$$

where $\Delta = \left[\frac{\alpha}{\alpha\mathbf{x}}, \frac{\alpha}{\alpha\mathbf{y}}\right]$ and $\Delta = \Delta\cdot\Delta = \frac{\partial^2}{\partial\mathrm{x}^2} + \frac{\partial^2}{\partial\mathrm{y}^2}$. For uniform depth, this simplifies further to the Laplace equation $\Delta\Phi = 0$. We reduce the number of parameters by normalizing distance by $\mathrm{w_s}$ and time by $\mathrm{w_s}/\mathbf{u}_{\text{in}}$ so that

$$\Phi = \mathbf{u}_{\text{in}}\mathrm{w_s}\Phi \qquad \vec{\mathbf{u}} = \mathbf{u}_{\text{in}}\vec{u}, \qquad \vec{\mathbf{x}} = \mathrm{w_s}\vec{x}, \qquad \Delta = \frac{1}{\mathrm{w_s}}\Delta. \qquad \Delta = \frac{1}{\mathrm{w_s^2}}\Delta. \tag{4}$$

Normalized, the governing equation is

$$\Delta\Phi = 0, \tag{5}$$

with the boundary conditions

$$\lim_{x\to-\infty} u = \lim_{x\to-\infty}\frac{\partial\Phi}{\partial x} = 1, \qquad \lim_{x\to+\infty}\Phi = 0, \tag{6a}$$

$$v|_{y=0} = \left.\frac{\partial\Phi}{\partial y}\right|_{y=0} = \alpha\, f, \qquad v|_{y=\frac{1}{\gamma}} = \left.\frac{\alpha\Phi}{\partial y}\right|_{y=\frac{1}{\gamma}} = 0. \tag{6b}$$

Herein, $\alpha = \mathbf{v}_0/\mathbf{u}_{\text{in}}$ is the relative strength of the flow into the side branch with respect to that along the main channel, and $\gamma = \mathrm{w_s}/\mathbf{w_0}$ is the ratio of the width of the inlet to that of the main channel. We fix Φ to zero at the downstream end of the main channel. The solution naturally adjusts to $\lim_{x\to+\infty} u = \lim_{x\to+\infty}\partial\Phi/\partial x = 1-\alpha\,\gamma$ at the downstream boundary.

As potential flow is linear, it can be decomposed into the sum of superimposed potential flows. This implies that the depth-averaged flow along the main channel does not influence the depth-averaged flow into the side branch and vice versa (figure 1). The potential flow can thus be determined by convolving the fundamental solution of the Laplacian with the velocity profile f. For the limit case of an infinitely wide main channel ($\mathbf{w_0}\to\infty, \gamma\to 0$), this is

$$\Phi = -x + \frac{\alpha}{\pi}\int_{-\frac{1}{2}}^{\frac{1}{2}} f(x')\log\sqrt{(x-x')^2+y^2}\mathrm{d}x'. \tag{7}$$

This yields the first important result, namely, that for a wide main channel and a particular velocity profile f; the depth-averaged flow is fully determined by a single parameter α, irrespectively of scale.

There is an analytic solution when the velocity distribution f is a piecewise continuous polynomial. In particular, for a constant profile ($f = 1$, when $-\frac{1}{2}\le x\le+\frac{1}{2}$, and 0 otherwise), the velocity is

$$u = 1 - \frac{\alpha}{2\,\pi}\ln\left(\frac{1+4\,x^2+4\,y^2+4\,x}{1+4\,x^2+4\,y^2-4\,x}\right), \tag{8a}$$

$$v = \begin{cases} -\frac{\alpha}{\pi}\,\mathrm{arctan2}\left(4\,y,\ 4\,x^2+4\,y^2-1\right), & y>0, v_0, \\ & y=0. \end{cases} \tag{8b}$$

Herein, arctan2 is the unambiguous two-argument arctangent with the range of the full circle of $2\,\pi$. In the vicinity and far away from the bifurcation, the velocity asymptotically assumes simpler forms, which we consider hereafter.

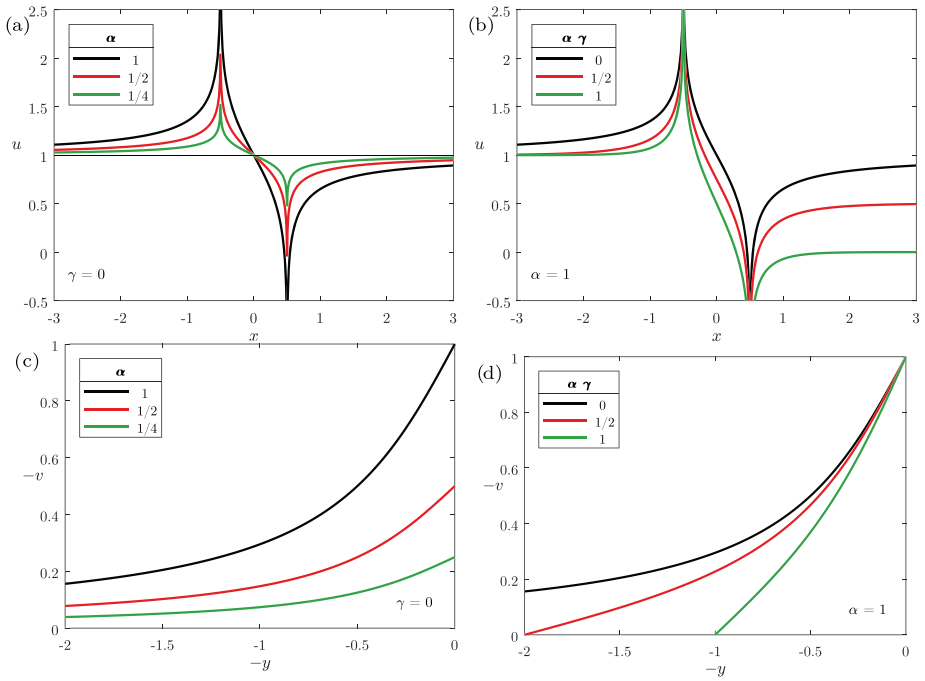

Figure 2. (a and c) Velocity at the diversion from a wide channel ($\gamma = 0$) depending on the strength of the outflow α, as given by equations (8a) and (8b); (a) in the direction of the main channel along the diversion $u(x, 0)$, inflow is from the left; and (c) across the main channel at the centre of the diversion $v(0, y)$, outflow into the side branch is at the right; (b and d) velocity at a diversion depending on the main channel width γ, for unit outflow velocity ($\alpha = 1$), as given by equations (11a) and (11b).

The linearized velocity near the centre of the diversion $(x, y) = (0, 0)$ is

$$u = 1 - \frac{4\,\alpha\,x}{\pi}, \qquad v = \alpha\left(1 + \frac{4\,y}{\pi}\right), \tag{9}$$

which is valid within the circle spanned around the center with the radius $\frac{1}{2}$.

The velocity component in the direction of the main channel thus decreases linearly along the diversion, and the transverse velocity directed toward the side branch increases linearly toward the diversion (Figures 2a and 2b). The velocity in the direction of the main channel u does not change across the main channel at the centre of the diversion.

With increasing distance from the diversion, the velocity approaches the hyperbolic asymptotes

$$u = 1 - \frac{\alpha\,x}{\pi\,(x^2 + y^2)}, \qquad v = \frac{\alpha\,y}{\pi\,(x^2 + y^2)}. \tag{10}$$

Far from the diversion, the velocity is thus identical to that caused by the outflow at a single point and therefore depends neither on the width nor on the velocity profile along the diversion.

The flow along the main channel is symmetric with respect to the mean velocity, that is, $u_0 - u(x, y) = u(-x, y) - u_0$, $u_0 = 1$. The approaching flow accelerates toward the diversions (equation (10)) and then rapidly decreases along the diversion (equation (9) and Figure 2a) and recovers to the free stream velocity downstream of the diversion (equation (10)). The flow across the main channel is likewise symmetric, that is, $v(x, y) = v(-x, y)$. It decreases linearly across the main channel, close to the diversion (equation (9)), and vanishes asymptotically (equation (9) and Figure 2b). The velocity along the main channel has two poles; that is, it spikes toward infinity at the downstream end and toward negative infinity at the upstream end of the diversion. There is thus a stagnation point at the bank downstream of the diversion, where the velocity is zero.

2.2. Flow at a Lateral Diversion From an Arbitrarily Wide Channel

Let $g_u(x, y, y_0)$ and $g_v(x, y, y_0)$ be the generalized expressions of equations (8a) and (8b) for the velocity in a wide channel ($\mathbf{w_0} \to \infty$), where the origin is shifted to y_0 along the axis across the main channel, then the velocity for a finitely wide main channel is given by the series

$$u = \left(1 - \frac{1}{2}\gamma\ \alpha\right) + \sum_{k=-\infty}^{\infty} g_u\left(x, y, \frac{2\,k}{\gamma}\right), \tag{11a}$$

$$v = \sum_{k=-\infty}^{\infty} g_v\left(x, y, \frac{2\,k}{\gamma}\right). \tag{11b}$$

The boundary conditions at the left and right banks are satisfied, as v (equation (8b)) is point symmetric ($v(x, y) = -v(x, -y)$. At the right bank ($y = 0$), the terms for $k \neq 0$ cancel so that $v(x, 0) = g_v(x, y, 0)$. At the opposite bank $\left(y = \frac{1}{\gamma}\right)$, all terms of the series of v cancel, so that $v\left(x, \frac{1}{\gamma}\right) = 0$.

Equations (11a) and (11b) are the general solution for junction flow. For $\alpha\,\gamma > 1$, the junction resembles a confluence where the flow enters the side branch from both sides of the main channel, and for $\alpha < 0$, the junction resembles a confluence, where the flow from the side branch joins the main channel. For $\gamma < 0$, the flow in the main channel is directed from right to left.

Near the center ($(x, y) = (0, 0)$) of the diversion, the velocity is

$$u = \left(1 - \frac{1}{2}\alpha\ \gamma\right) + \alpha\ \gamma\ \coth\left(\frac{\pi\ \gamma}{4}\right) x, \tag{12a}$$

$$v = \alpha - \alpha\ \gamma\ \coth\left(\frac{\pi\ \gamma}{4}\right) y. \tag{12b}$$

The mean velocity $u_0 = \left(1 - \frac{1}{2}\gamma\ \alpha\right)$ at the bifurcation center decreases with the main channel width. The magnitude of the gradient of the velocity increases slightly with the main channel width. However, even for the case that all water is diverted ($\alpha\,\gamma = 1$), the gradient is only 20% larger compared to the case where the same amount of water is diverted from an infinitely wide channel.

In the far field, where $r^2 = x^2 + y^2 \gg \frac{1}{4}$,

$$u = \left(1 - \frac{1}{2}\alpha\ \gamma\right) + \frac{\alpha\ \gamma}{2}\frac{x}{r}\ \coth\pi\ \frac{\gamma}{2}\ r, \tag{13}$$

$$v = \frac{a\ \gamma}{4}\ \left(\cot\pi\frac{\gamma}{2}\ r^- + \cot\pi\frac{\gamma}{2}\ r^+\right), r^{\pm} = (y \pm i\ x). \tag{14}$$

The upstream influence of the bifurcation decays more rapidly when the main channel is narrower (Figure 2b). Conversely, the flow accelerates more rapidly in the vicinity of the bifurcation, when the main channel is narrower. Likewise, v, the velocity component in the direction of the side branch, decreases more rapidly across the main channel, the narrower its width so that the velocity reaches zero at the opposite bank (Figure 2d).

2.3. Velocity of the Near-Bed Flow

The steering of sediment by secondary flow is crucial for the division of sediment at lateral diversions. As the flow turns into the side branch, it generates a centrifugal force. The force is outward directed with respect to the direction of turning. This force is balanced by an inward-directed pressure gradient, which is generated by a water surface slope perpendicular to the streamlines (Rozovskii, 1957). However, the forces are only balanced in a depth-averaged sense. In the upper part of the water column, the net force is directed outward, while it is directed inward near the bed, as the centrifugal force decreases with the magnitude of the flow velocity from the water surface to the bed, while the pressure gradient is nearly constant throughout the water column. This directs the near-bed flow more toward the diversion, and the near-surface flow more toward the main channel. The velocity of the flow near the bed can be approximated as (Rozovskii, 1957)

$$\vec{\mathbf{u}}_b = \vec{\mathbf{u}} + f_s\frac{\mathbf{h}}{\mathbf{R}}\begin{pmatrix}\mathbf{v}\\ -\mathbf{u}\end{pmatrix}, \tag{15}$$

where $\mathbf{R}$ is the radius of curvature of the streamlines of the depth-averaged flow, C is the Chezý coefficient, and $f_s = 11.9\left(1 - \frac{7.6}{C}\right)$ is the secondary flow scale (De Vriend, 1977). The value of f_s is approximately 11 for sand-bed rivers where the roughness is low, but lower in small channels and flumes. The relation (15) does not account for the adaptation of the secondary flow due to changes in curvature (Kalkwijk & Booij, 1986). The neglected adaptation will only cause a small difference for the case of rivers, where the channel width is typically much larger than the depth.

Expressed in the nondimensional quantities, the velocity near the bed is

$$\vec{u}_b = \vec{u} + \beta \frac{1}{R}\begin{pmatrix} v \\ -u \end{pmatrix}, \tag{16}$$

where $\beta = f_s \frac{\mathbf{h}}{\mathrm{w_s}}$. The normalized curvature $\frac{1}{R} = \frac{\mathrm{w_s}}{\mathbf{R}}$ is (De Vriend, 1977)

$$\frac{1}{R} = \frac{1}{|\vec{u}|^3}\left(\frac{\partial v}{\partial x}u^2 + \left(\frac{\partial v}{\partial y} - \frac{\partial u}{\partial x}\right)u\,v - \frac{\partial u}{\partial y}v^2\right) = \frac{1}{|\vec{u}|}\frac{\partial v_t}{\partial x_t}, \tag{17}$$

where $|\vec{u}| = \sqrt{u^2 + v^2}$ is the velocity magnitude, x_t is the distance along the tangent of the streamline, and v_t is the velocity component orthogonal to it. The curvature can be analytically determined from the velocity, but its expression is lengthy. However, it only depends on the parameters α and γ. The velocity near the bed is thus uniquely determined by the relative strength of the diverted flow, α; the ratio of the width of the inlet to that of the side branch, γ; and the secondary flow scale, β. This carries over to the division of bedload, as it uniquely determined of by the streamlines of the near-bed flow.

3. Division of Sediment at a Lateral Diversion

In this section, we analyze how the predicted sediment division depends on the aforementioned parameters. We do this on hand of the water-to-sediment division ratio:

$$\frac{\mathbf{S_s}}{\mathbf{S_{in}}}\frac{\mathbf{Q_{in}}}{\mathbf{Q_s}} = \frac{\mathbf{c_s}}{\mathbf{c_{in}}} = \frac{\mathbf{w}_b}{\mathbf{w_0}} = \lim_{x\to-\infty}\frac{y_b}{y_d}, \tag{18}$$

where $\mathbf{c_{in}} = \frac{\mathbf{S_{in}}}{\mathbf{Q_{in}}}$ and $\mathbf{c_s} = \frac{\mathbf{S_s}}{\mathbf{Q_s}}$ are the pseudo sediment concentrations in the approaching and diverted channels, respectively. The water-to-sediment division ratio is equal to the ratio between the distances of the dividing streamlines of the near-bed (y_b) and the depth-averaged flow (y_d), at the upstream end of the main channel (Figure 1). For the depth-averaged flow, $\lim_{x\to-\infty} y_d = \alpha$, so that only y_b has to be found by integrating the streamline of the near-bed flow. We compare the sediment-to-water division ratio, because the sediment division ratio $\mathbf{S_s}/\mathbf{S_{in}}$ is ill-defined when the ratio of the width of the side branch to that of the main channel is small ($\gamma \to 0$) and because the sediment division $\mathbf{Q_s}/\mathbf{Q_{in}}$ is assumed to be known; hence, the sediment-to-water division ratio is the true quantity to be predicted.

3.1. Division of Bedload

As the division of bedload is demarcated by the dividing streamline of the near-bed flow, the division can be determined on hand of the dividing streamline. The amount of bedload $\mathbf{S_s}$ diverted to the side branch is

$$\mathbf{S_s} = \frac{\mathbf{w}_b}{\mathbf{w_0}}\mathbf{S_{in}}, \tag{19}$$

which is valid when the bedload rate is equal across the approaching channel and when the bed is not sloping across the approaching channel. $\mathbf{S_{in}}$ is the bed-material load in the approaching channel, and $\mathbf{w}_b = \mathrm{w_s}\lim_{x\to\infty} y_b$ is the distance of the dividing streamline of the near-bed flow (x_b, y_b) from the right bank, far upstream of the bifurcation.

Both the dividing streamline of the near-bed flow and the depth-averaged flow terminate in the stagnation point near the downstream end of the diversion (Figure 1). This allows us to determine $\mathbf{w}_b$ by a single integration of equation (16) backward in time, that is, backward from the stagnation point to a point far upstream to the diversion, where the influence of the diversion is negligible,

$$\vec{x}_b = \int_0^{-\infty} \vec{u}_b \mathrm{d}t, \vec{x}_b(0) = \vec{x}_s. \tag{20}$$

We advise on the numerical integration of the streamline in Appendix A.

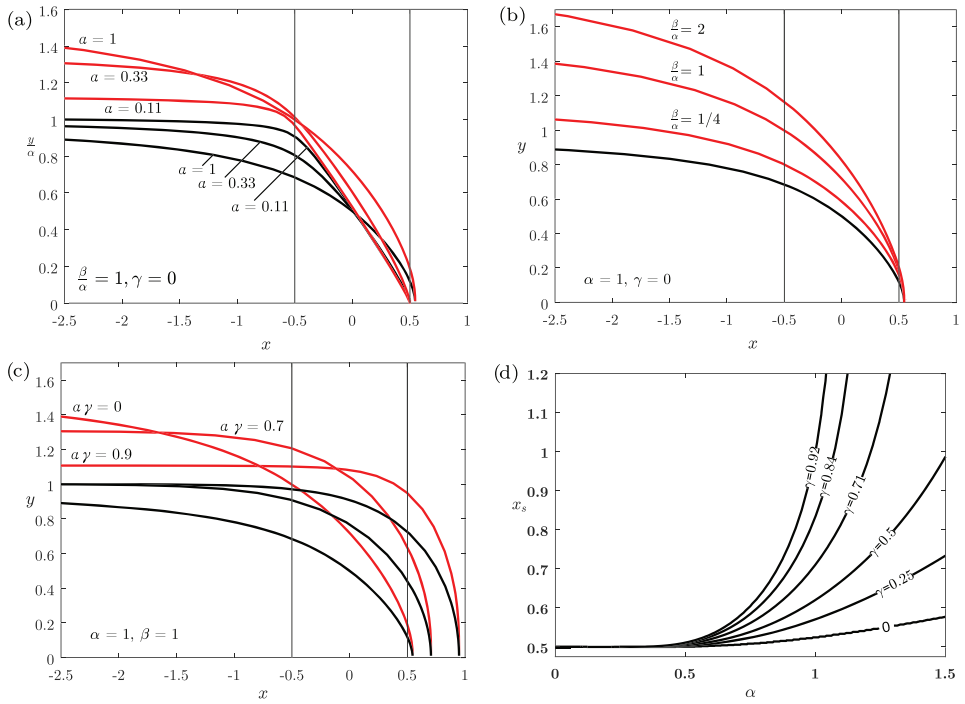

Figure 3. (a–c) Dividing streamline of the depth-averaged (black) and near-bed flow (red); vertical lines indicate the normalized width of the inlet to the side branch, (a) depending on the width of the side branch, (b) depending on the channel depth, and (c) depending on the discharge division; (d) position of the stagnation point $\vec{x}_s$

3.2. Division of Suspended Load

Sediment is transported in suspension when the shear stress is much larger than the threshold of motion. Such conditions are typical for sand-bed rivers (Schumm, 1985). Since the strength of the secondary flow decreases toward mid-depth and its direction changes into the opposite direction in the upper half of the water column, suspended load is divided more equally at lateral diversions than bedload (Dancy, 1947). The pathway of suspended sediment is not planar as the sediment is steered by vertical velocity and local imbalance of turbulence and settling. However, the bulk of bed material sand is typically suspended in the lower part of the water column, which suggests that a modified form of equation (15) can be adopted. We suggest, to determine the division of suspended sediment based on the dividing streamline at the distance $\bar{\mathbf{z}}$ above the bed, where the sediment flux is equal to the equilibrium depth-averaged flux in stationary uniform flow:

$$\vec{\mathbf{u}}_{ss} = \vec{\mathbf{u}} + f_s \frac{\mathbf{h} - 2\bar{\mathbf{z}}}{\mathbf{R}} \begin{pmatrix} \mathbf{v} \\ -\mathbf{u} \end{pmatrix} \tag{21}$$

so that $\beta = \left(1 - 2\frac{\bar{\mathbf{z}}}{\mathbf{h}}\right) f_s \frac{\mathbf{h}}{\mathrm{w_s}}$. As the suspended load only modifies the parameter β, it does not increase the parameter space. This is based on the observation that the strength of the secondary flow changes approximately linearly along the vertical. $\bar{\mathbf{z}}$ can be readily computed on hand of standard formulas for the velocity and suspended sediment concentration, such as a logarithmic velocity profile and a Rouse suspension profile (Vanoni, 2006).

3.3. Dividing Streamlines

The streamline of the near-bed flow takes a wider turn than the depth-averaged flow (Figure 1d). How much wider the turn is is determined by two factors: the secondary flow scale β and the curvature of the streamline $1/R$ (equation (16)).

Figure 3a shows the influence of the width of the inlet to the side branch on the division of sediment. For a narrow inlet, both α and β are small. When the inlet is narrow, then the streamline of the depth-averaged flow takes a single turn. When the inlet is wide, then the streamline becomes nearly straight with a single

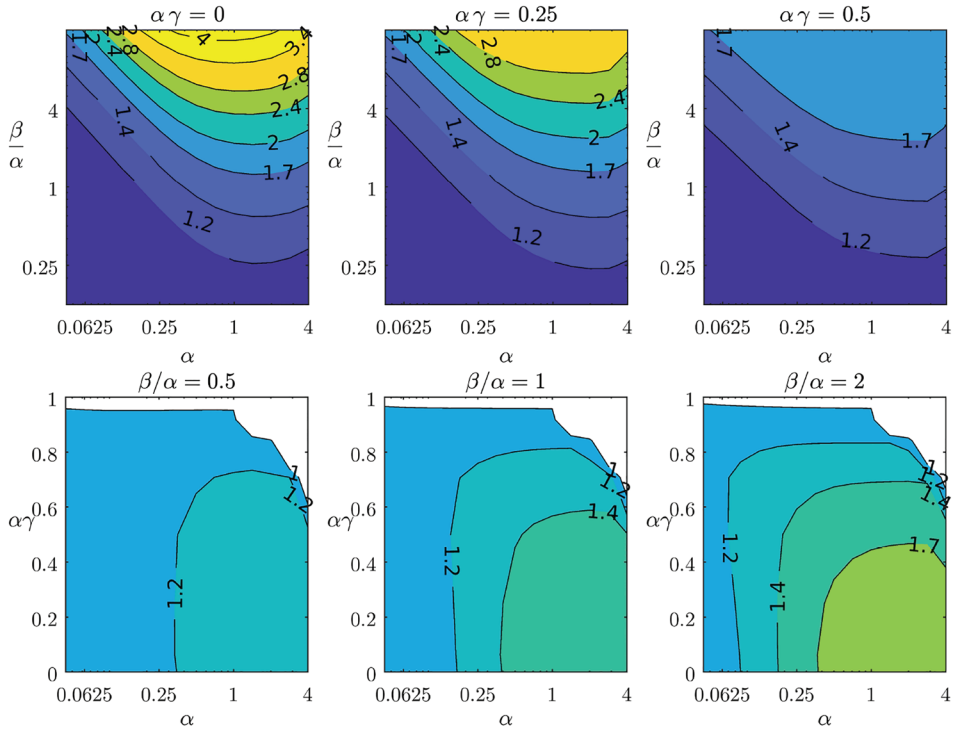

Figure 4. Sediment division ratio depending on the strength of the diverted flow $\alpha = \mathbf{v}_s/\mathbf{u}_0$ and depth of the main channel $\beta/\alpha = \mathbf{f}_s\,\mathbf{h}$ and different discharge division ratios $\alpha\,\gamma = \mathbf{Q}_s/\mathbf{Q}_{in}$.

knick point near $\vec{x} = \left(-\frac{1}{2}, \alpha\right)$. As a consequence of the stronger curvature for a narrower inlet, the dividing streamline of the near-bed flow takes a wider turn, so that the sediment-to-water division ratio is higher.

Figure 3b shows the influence of the channel depth, which is proportional to β, on the division of sediment. As the strength of the secondary flow increases with the depth, the dividing streamline of the near-bed flow takes a larger turn further away from the side branch so that the sediment-to-water division ratio is higher.

Figure 3c shows the influence of the discharge division ($\alpha\,\gamma$) on the division of sediment. The stagnation point moves further downstream when a larger fraction of the discharge is diverted (Figure 3d). Since the velocity downstream of the bifurcation is also lower for a higher fraction of diverted discharge, the secondary flow intensity is low as well. Hence, for a larger fraction of diverted discharge, or a narrower main channel for the same amount of diverted discharge, the dividing streamline of the near-bed flow thus takes a narrower turn, and the sediment-to-water division ratio is lower.

3.4. Influence of the Width, Depth, and Discharge Division

The channel width, depth, and discharge division affect several of the parameters α, β, and γ so that their relationship with the sediment division is not straightforward. When the width of the inlet to the side branch increases and the amount of diverted discharge remains constant, then α decreases, and β/α remains identical. Figure 4 shows that for this case the sediment-to-water division ratio decreases, that is, $\mathbf{c_s}/\mathbf{c_{in}}$ decreases with w_s, if $\mathbf{Q}_s$ remains the same. When the depth increases and the depth-averaged flow is identical, then α remains identical, and β/α increases. Figure 4 shows that for this case the sediment-to-water division ratio increases; that is, $\mathbf{c_s}/\mathbf{c_{in}}$ increases with $\mathbf{h}$, as long as $\mathbf{u}$, $\mathbf{v}$, w_s, and $\mathbf{w_0}$ remain the same. The dependence on the inlet width and depth is a direct consequence of their relation to the strength of the secondary flow (equation (15)), as the strength of the secondary flow increases both with the magnitude of the velocity and the depth of the channel.

When the width of the main channel increases, and the velocity and other geometrical properties remain the same, then α and β/α remain constant, and $\alpha\,\gamma$ decreases. Figure 4 shows that for this case the sediment-to-water ratio is not affected when α is small but increases when α is large. When α is not small,

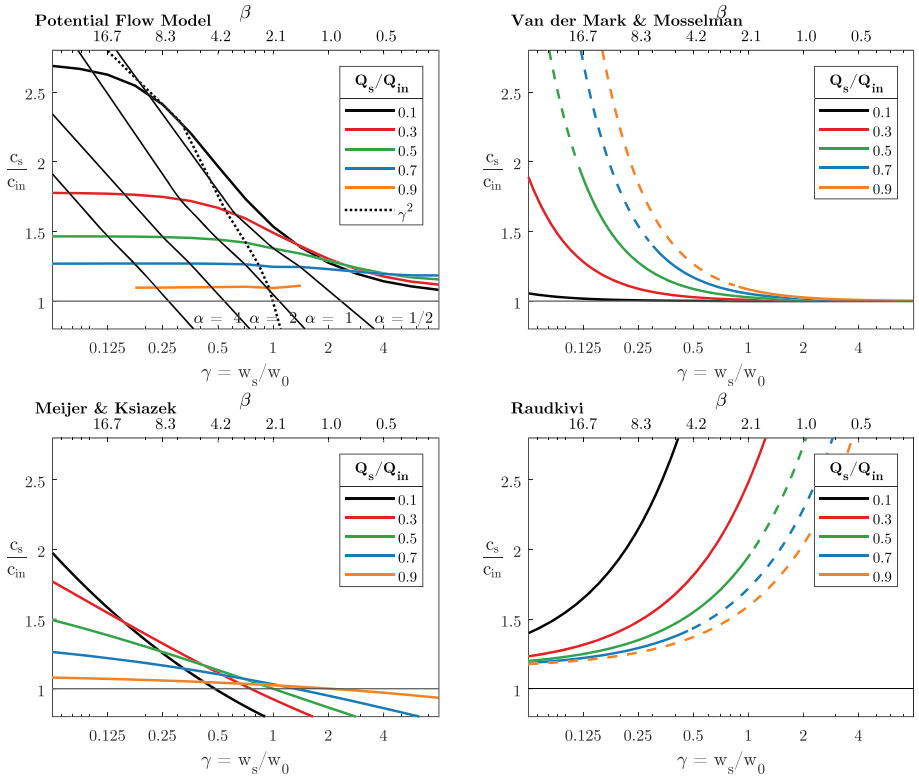

Figure 5. Sediment-to-water division ratio $\mathbf{c_s/c_{in}}$ depending on the discharge division and ratio of width between side and main branch. Depth $\mathbf{h}$ and specific discharge ($\mathbf{Q_{in}/w_0}$) in the approaching channel are kept constant. By (a) our potential flow model and the empirical relations by (b) van der Mark & Mosselman (c) Meijer & Ksiazek, and (d) Raudkivi. Infeasible predictions ($\mathbf{c_s}\ Q_s > \mathbf{c_{in}}\ Q_{in}$) are dashed. For the potential flow model, the width-to-depth ratio of the main channel was set to 25, similar to that at the Kapuas bifurcations (Kästner et al., 2017). α varies diagonally through the plot (bold). The dashed line indicates the values for the hydraulic geometric relationship of $\gamma = w_s/\mathbf{w_0} = (Q_s/Q_{in})^{1/2}$.

$\mathbf{c_s/c_{in}}$ increases with $\mathbf{w_0}$, as long as $\mathbf{u}_0$, $\mathbf{v}_0$, w_s, and $\mathbf{h}$ remain constant. This relation ensures the conservation of mass for the case when the entire discharge is diverted, as $\mathbf{c_s} \rightarrow \mathbf{c_{in}}$, when $\alpha\,\gamma \rightarrow 1$. Note that, in general, the pseudo concentration in the side branch is larger than in the approaching channel, except for the limit cases where it is equal.

When the amount of diverted discharge increases, but the channel geometry remains constant, then α and $\alpha\,\gamma$ increase, but β remains the same. Figure 5 shows that for this case the sediment-to-water division ratio is not a monotonous function. The sediment-to-water division ratio decreases with the fraction of diverted discharge when the inlet to the side branch is wide (i.e., γ is large), but it increases with the fraction of diverted discharge, when the inlet is relatively narrow (i.e., γ is small).

4. Discussion

4.1. Stability of Fluvial Channel Networks

The division of sediment at river bifurcations is relevant for the stability of deltaic and anastomosing channel networks. Wang et al. (1995) showed that for a stable configuration where both branches remain open, proportionally less sediment than water has to be diverted into the smaller branch. This corresponds to a sediment-to-water division ratio that is less than unity ($\mathbf{c_s} < \mathbf{c_{in}}$). However, the potential flow model predicts that the sediment-to-water division ratio is always larger than unity, which is in agreement with scale experiments (Bulle, 1926; Habermaas, 1935; Herrero et al., 2015; Riad, 1961). Side branches will thus fill in over time, if there are no additional factors than the channel width and depth that reduce the sediment-to-water division ratio. Bolla Pittaluga et al. (2003,2015) showed that a transverse slope across the approaching channel can stabilize symmetric bifurcations, by steering sediment preferentially in the larger and thus deeper branch. However, at lateral diversions, the bed is typically scoured at the downstream end of the inlet to

the side branch (Kästner & Hoitink, 2019; Önen & Agaccioglu, 2013; Herrero et al., 2015). This likely steers sediment toward and not away from the lateral branch.

When a branch fills in, it will receive a lower fraction of water but also become narrower over time. A reduction of discharge and inlet width has the opposite effects on the water-to-sediment division ratio when a small fraction of discharge is diverted (Figure 5a). How the sediment-to-water division ratio changes with the channel size can be uniquely determined with help of empirical hydraulic geometry, according to which the width of channels is approximately proportional to the square root of the discharge that they receive (Eaton, 2013). When the channel width is predicted by the empirical hydraulic geometry, then the sediment-to-water division ratio increases with the discharge over time (Figure 5a). This would accelerate the rate of closure of a side branch over time. However, the inlet of the side branches can be wider than the side branch further downstream. Bulle (1926) already noticed that smoothing of the diversion corners and the coincidental increase of the inlet area reduce the amount of the diverted sediment in scale experiments. Similarly does the inlet width effectively increase, when the side branch takes off at an angle that is larger or smaller than 90°. To fully understand how the division of sediment influences the morphodynamics of channel networks, it is thus necessary to study how the width and geometry of the inlet evolve.

4.2. Empirical Prediction of Sediment Division

In this section, we analyze several empirical relations for the division of sediment that have been previously suggested and compare those to predictions by our model. The existing empirical relations typically focus on the ratio of the diverted and the approaching flux of sediment $\mathbf{S_s}/\mathbf{S_{in}}$ depending on the ratio of the diverted to the approaching discharge $\mathbf{Q_s}/\mathbf{Q_{in}}$. We compare the models based on the predicted sediment-to-water division ratio $\mathbf{c_s}/\mathbf{c_{in}} = \mathbf{S_s}/\mathbf{S_{in}}\,\mathbf{Q_{in}}/\mathbf{Q_s}$, for the reasons outlined in section 3.

Raudkivi (1993) gives the relation

$$\frac{\mathbf{w}_b}{\mathrm{w_s}} = a_b + b_b\,\alpha, \tag{22}$$

where $\mathbf{w}_b$ is the width of the diverted flow near the bed in the upstream channel and $a_b \approx 0.4$ and $b_b \approx 1.15$ are empirical parameters. This is equivalent to a sediment-to-water division ratio of

$$\frac{\mathbf{c_s}}{\mathbf{c_{in}}} = a_b \frac{1}{\alpha} + b_b. \tag{23}$$

Meijer and Ksiazek (1994) conducted numerical experiments for a diversion with idealized geometry. They suggest two relations. The first one is

$$\frac{\boldsymbol{S_s}}{\left(\boldsymbol{S_s} - \boldsymbol{S_{in}}\right)} = k_0 + k_1 \frac{\boldsymbol{Q_s}}{\left(\boldsymbol{Q_{in}} - \boldsymbol{Q_s}\right)}, \tag{24}$$

with the empirical values $k_1 = 2.63$, and $k_0 = -0.1$ for the deflection of bedload at a 90° diversion. The relation is only asymptotically consistent when $k_0 = 0$ (Wang et al., 1995). In this case, the relation simplifies to

$$\frac{\mathbf{c_s}}{\mathbf{c_{in}}} = k_1\left(1 + \left(k_1 - 1\right)\alpha\,\gamma\right)^{-1}. \tag{25}$$

As this relation does not account for the width-ratio of the channels, we do not consider it further. The second relation proposed by Meijer and Ksiazek (1994) is the power law

$$\frac{\mathbf{S_s}}{\mathbf{S_{in}} - \mathbf{S_s}} = \left(\frac{\mathbf{Q_s}}{\mathbf{Q_{in}} - \mathbf{Q_s}}\right)^m \left(\frac{\mathbf{w_0}}{\mathrm{w_s}}\right)^n, \tag{26}$$

with the empirical values $m = 1.15$ and $n = -0.71$. The relation is asymptotically only consistent for $m+n = 1$ (Wang et al., 1995). For a bifurcation with a horizontal bed and a constant width of the main channel, the relation is identical to a sediment-to-water division ratio of

$$\frac{\mathbf{c_s}}{\mathbf{c_{in}}} = \alpha\,\gamma\left(1 + \gamma^{-n}\left(\frac{1 - \alpha\,\gamma}{\alpha\,\gamma}\right)^{-m}\right)^{-1}. \tag{27}$$

For a wide main channel with $m + n = 1$, this asymptotically approaches

$$\frac{\mathbf{c_s}}{\mathbf{c}_{\text{in}}} = \alpha^{m-1}. \tag{28}$$

The potential flow model suggests $m > 1$, which was the case for the value fit by Meijer and Ksiazek (1994) to their experimental data. Wang et al. (1995) derived stability criteria for symmetric bifurcations depending on the parameter m and the degree of nonlinearity of the sediment transport formula.

Van der Mark and Mosselman (2013) determine the sediment division by the sophisticated relation:

$$\frac{\mathbf{S_s}}{\mathbf{S}_{\text{in}}} = \frac{\mathbf{Q_s}}{\mathbf{Q}_{\text{in}}} + \left(c \frac{\mathbf{Q_s}}{\mathbf{Q}_{\text{in}}} \frac{\mathbf{w_0}}{\mathrm{w_s}} \right)^{b/3} \frac{\mathbf{R}}{\mathbf{w_0}} \theta \left(\frac{1}{\cos \delta} - 1 \right), \tag{29}$$

where c is a constant, b the degree of nonlinearity of the sediment transport, and θ, $\mathbf{R}$, and δ depend on the channel geometry and flow conditions as specified by Van der Mark and Mosselman (2013). The corresponding sediment-to-water division ratio is, with θ, R, and δ being functions of α and β,

$$\frac{\mathbf{c_s}}{\mathbf{c}_{\text{in}}} = 1 + c^{b/3} \alpha^{(b/3-1)} \frac{\mathbf{R}}{\mathrm{w_s}} \theta \left(\frac{1}{\cos \delta} - 1 \right). \tag{30}$$

4.3. Comparison of the Potential Flow Model to Empirical Predictions

Figure 5 shows the predicted sediment-to-water division ratio depending on the relative width of the side branch, parameterized by $\gamma = \mathrm{w_s}/\mathbf{w_0}$, and discharge division ratio $\mathbf{Q_s}/\mathbf{Q}_{\text{in}}$. The parameter α varies dynamically through the diagram, indicated by diagonal lines in Figure 5a. There is one free parameter, which is the width to depth ratio of the approaching channel. We set this to 50, which is in the range of width-to-depth ratios in large rivers (Kästner et al., 2017). β varies inverse proportionally to γ.

We find that the three empirical relations disagree among each other regarding how the sediment-to-water division ratio depends on the channel geometry and discharge division. None of the relations agrees with the predictions by our potential flow model. This raises the question which of the predictions is closest to reality. In this respect, we find that the relations proposed by Raudkivi (1993) and Van der Mark and Mosselman (2013) predict for certain parameter combinations that more sediment is diverted to the side branch than what is incoming through the approaching channel. This seems implausible (dashed lines in Figures 5b and 5d). The model by Van der Mark and Mosselman (2013) predicts the sediment-to-water division ratio to decrease with the inlet width, and the concentration in the diverted channel to be larger than in the approaching channel $\mathbf{c_s}/\mathbf{c}_{\text{in}} > 1$ (Figure 5b). Both those predictions are in agreement with the potential flow model. The model by Van der Mark and Mosselman (2013) also predicts that the sediment-to-water division ratio increases with the fraction of the diverted discharge, irrespective of the channel width. This is not in agreement with the potential flow model, which only predicts the sediment-to-water division ratio to increase with the fraction of diverted discharge when the inlet to the side branch is wide. Note that exactly, this discrepancy leads to implausible predictions for the cases when the fraction of the diverted discharge is large and the inlet is narrow.

The relation by Meijer and Ksiazek (1994) predicts the sediment-to-water division ratio to decrease with the width of the inlet to the side branch. It also predicts the sediment-to-discharge division to increase with the fraction of diverted discharge when the inlet to the side branch is wide and to decrease with the fraction of the diverted discharge when the inlet to the side branch is narrow. These predictions all agree with that of the potential flow model. From the perspective of this qualitative comparison, the predictions by Meijer and Ksiazek (1994) are the closest to our potential flow model, in comparison to the other empirical relations. The predictions by Meijer and Ksiazek (1994) are also physically plausible for any parameter combination. However, the conclusion that the predictions by Meijer and Ksiazek (1994) is, in general, more reliable than the other relations would be premature, as Meijer and Ksiazek (1994) based their relation on numerical simulations in a channel with idealized geometry and a flat bed. These are close to the idealized geometry assumed by us and does not necessarily hold in canals and rivers.

The relation by Meijer and Ksiazek (1994) predicts overall a lower sediment-to-water division ratio than the potential flow model. This can be explained by the fact that Meijer and Ksiazek (1994) did not include a correction for suspended load in their relation, although a large fraction of the sediment was transported in their simulation as suspended load. The relation by Meijer and Ksiazek (1994) predicts sediment-to-water

division ratios smaller than one for a wide channel, which is not the case for the potential flow model. This could be a misfit in the relation by Meijer and Ksiazek (1994), as their data set does not include simulations for wide inlets, but it could also indicate a limitation in our potential flow model, due to the local expansion of the main channel flow into a wide inlet.

The relation by Raudkivi (1993) predicts the sediment to water division ratio to increase with the inlet to the side branch and to decrease with the fraction of the diverted discharge. The predicted sediment-to-water division ratios are implausible for cases where a large fraction of the discharge is diverted and the inlet to the side branch is wide.

We think that the discrepancy between the predictions by empirical models is caused by underlying data sets, which each cover only a small part of the space spanned by the parameters α, β, and γ. In particular, the width-to-depth ratio in scale experiments is typically much smaller than in real rivers, and the channel width is for practical reasons kept constant, so that the influence of the channel geometry cannot be reliably inferred.

4.4. Toward a Generic Understanding of the Sediment Division

Our results indicate that most likely, no simple closed-form expression for the division of sediment at lateral diversions exists, at least not an expression as simple as the ones that have been previously suggested. We think that the sediment division is best predicted by a high-complexity numerical model for particular applications (Gaweesh & Meselhe, 2016). For the general case, further insight could be gained by a model that is still idealized but incorporates more complex processes than our simple potential flow model.

Our model strongly simplifies the geometry of the bifurcation and determines the flow into the side branch by a predefined velocity profile, without explicitly including the side branch into the computational domain. This neglects the feedback of the flow within the side branch on the division. This feedback can be important when the flow in the side branch separates (Constantine et al., 2010; Ramamurthy et al., 2007). The separation bubble effectively reduces the inlet width, and thus the amount of the diverted discharge and sediment. The contraction coefficient has to be considered for the design of artificial diversions. At alluvial bifurcations, flow separation can occur for a short period after a bifurcation is formed, that is, by a chute cutoff or an avulsion event. However, the banks align over time with the streamlines, so that the flow does not separate any more. Indeed, the flow does not separate within the side branches of the Kapuas, despite their large angles at which they branch off (Kästner & Hoitink, 2019). The representation of the flow by a velocity profile is therefore reasonable.

Apart from the geometry, the most relevant simplification in our model is that the velocity distribution f of the flow across the diverted channel is uniform. This is exact when there is free flow over a side weir, where the diverted flow is critical. In the case of subcritical flow, the velocity profile is the result of several processes. First, the flow that turns at the upstream end of the bifurcation has a slope advantage with respect to the flow that turns at the downstream end. Second, the secondary flow advects momentum toward the downstream end of the bifurcation. Third, the streamlines are continuous and thus follow the direction of the banks of the approaching channel, when the channels meet at a sharp corner. Scale experiments show that, altogether, the strength of the flow increases along the diversion (Kawai et al., 1993). We argue that nonuniformity of f only affects our results qualitatively and does not change the overall trend with respect to the inlet size and discharge division. The secondary flow is stronger either when the inlet is narrower, or when more discharge is diverted into the inlet, irrespective of the velocity distribution across the diversion.

The second most relevant simplification in our model is that it does not account for the local imbalance between the friction and pressure gradient. Potential flow is valid when the friction can be neglected from the momentum balance. Friction is important for the separation of the flow and recirculation in the inlet to the side branch, when the channels meet at a sharp corner. However, the division of sediment is determined by the flow in the approaching channel, which is only indirectly influenced by the recirculation within the side branch. At natural river bifurcations, there is also a smooth transition between the channels without sharp corners. This inhibits the formation of a recirculation cell. Observations of this phenomenon at bifurcations of the Kapuas River have motivated us to undertake this study (Kästner & Hoitink, 2019).

High-complexity numerical experiments may yield additional insights into the subtle effects that friction may have. Since including the effect of friction weakens the assumptions, this will lead to a more robust and accurate prediction than that of the potential flow model. However, the fundamental disagreement

between the empirical relations could indicate that complex processes like migrating bedforms influence the division of sediment, which are difficult to reproduce even with a high-complexity numerical model, and which would best be addressed with physical experiments. Our nondimensional analysis can aid the design of both computational and physical experiments that can further explore the diversion of sediment into lateral branches of lowland rivers.

5. Conclusion

We present a mathematical analysis of the division of sediment at open channel bifurcations where one channel branches off to the side. We show that for such a lateral diversion with idealized geometry with a flat bed and rectangular channels, the depth-averaged flow is uniquely determined by only two parameters. One corresponds to the strength of the flow into the side branch, and the other to the ratio of the width of the side branch to that of the main channel. We show that the division of sediment, in turn, is uniquely determined in combination with a third parameter, which scales with the water depth. We find that for the same amount of diverted discharge, the sediment-to-water division ratio decreases with the width of the inlet to the side branch and increases with the water depth. This suggests that the morphodynamics of fluvial channel networks is influenced by the local morphology of the inlet to the side branch.

Our model also shows that the relation between the discharge division and sediment-to-water division ratio is complex. The sediment-to-water division ratio increases with the fraction of diverted discharge when the inlet to the side branch is wide but decreases with the discharge when the inlet to the side branch is narrow. A comparison of previously published empirical relations shows that there is no agreement on how the sediment-to-water division ratio depends on the fraction of the diverted discharge. None of the empirical relations sufficiently agrees with the predictions by our simple model. This suggests that further research is required to clarify the division of sediment at strongly asymmetric bifurcations where a small channel branches off to the side.

Appendix A: Numerical Computation of the Streamline

The dividing streamline of the near-bed flow can be determined by backward integration. We recommend an ODE solver for stiff systems that is available in modern high-level programming environments. In addition to the velocity vector $\vec{u}_b$, the solver should be supplied with the Jacobian $\frac{\partial u_{b,i}}{\partial x_i}$ for reliable evaluation. As for the streamline, only the direction of the velocity is relevant, but not its magnitude; the parallel computation of multiple streamlines can be accelerated by normalizing the velocity.

For integration, the user has to make two choices: first, at which point upstream of the bifurcation the integration of the streamline (20) is stopped and, second, after how many terms the series (11a) and (11b) is truncated. The integration can be stopped when the flow is close to parallel to the x axis. The error introduced by stopping the integration at a finite distance from the origin can be approximated by integrating the streamline (20) along $y = \alpha$, with $u \approx 1$ and v given by the far-field approximation (10) for a wield channel. A relative tolerance of $\epsilon = y_s(x)/\alpha - 1$ is achieved, when

$$x \gtrsim \frac{\alpha}{3\,\pi\,\epsilon}. \tag{A1}$$

For a narrow main channel, the desired accuracy is already reached at a much shorter distance.

In the far field, the truncation of the series at $k = \pm n$ introduces a relative error to the velocity of

$$\frac{u_n - u_{\inf}}{\alpha} \approx 2\sum_{k=n}^{\infty} \frac{x\,\gamma^2}{\pi\,4\,k^2} \approx \frac{x\,\gamma^2}{\pi\,2\,n}. \tag{A2}$$

More terms are required to achieve the desired accuracy when either the width-ratio γ or the distance x from the origin is large.

Acknowledgments
This research was supported by the Royal Netherlands Academy of Arts and Sciences (KNAW) Project SPIN3-JRP-29 as well as the Global Rivers programme of the Earth Observatory of Singapore and the Asian School of the Environment. FAIR data policy statement: All figures and tables can be directly reproduced from the equations presented in this manuscript. The flow and sediment division can be computed on-demand with a servlet that is hosted by the first author (at www.riverdolphin.xyz/lateral-diversion). The source code can be downloaded at GitHub (https://github.com/karlkastner).

References

Bateman, A., Medina, V., Coliles, A., Loaiza, A., García, W., & Puig, C. (2009). The impressive case of the uncontrolled diversion of the Patía River at its delta and the social and environmental consequences. In *Proceedings of the Congress of River, Coastal and Estuarine Morphodynamics (RCEM 2009)*. London: Taylor & Francis.

Bolla Pittaluga, M., Coco, G., & Kleinhans, M. G. (2015). A unified framework for stability of channel bifurcations in gravel and sand fluvial systems. *Geophysical Research Letters*, *42*, 7521–7536. https://doi.org/10.1002/2015GL065175

Bolla Pittaluga, M., Repetto, R., & Tubino, M. (2003). Channel bifurcation in braided rivers: Equilibrium configurations and stability. *Water Resources Research*, *39*, 3.

Bulle, H. (1926). Untersuchungen über die Geschiebeableitung bei der Spaltung von Wasserläufen: Modellversuche aus dem Flussbaulaboratorium der Technischen Hochschule zu Karlsruhe. Berlin: VDI-Verlag.

Buschman, F. A., Hoitink, A. J. F., Van der Vegt, M., & Hoekstra, P. (2010). Subtidal flow division at a shallow tidal junction. *Water Resources Research*, *46*, W12515. https://doi.org/10.1029/2010WR009266

Constantine, J. A., Dunne, T., Piégay, H., & Mathias Kondolf, G. (2010). Controls on the alluviation of oxbow lakes by bed-material load along the Sacramento River, California. *Sedimentology*, *57*(2), 389–407.

Dancy, A. G. (1947). *Stream sedimentation in a divided channel*. Ames, IA: Iowa State University.

De Heer, A., & Mosselman, E. (2004). Flow structure and bedload distribution at alluvial diversions, *River Flow* (Vol. 2004, pp. 801–806). Leiden: A.A. Balkema Publishers.

De Vriend, H. J. (1977). A mathematical model of steady flow in curved shallow channels. *Journal of Hydraulic Research*, *15*(1), 37–54.

Doets, I. J. E. (2015). The effect of islands in the Río Magdalena on discharge and sediment transport into the Canal del Dique, Colombia.

Dutta, S., Wang, D., Tassi, P., & Garcia, M. H. (2017). Three-dimensional numerical modeling of the Bulle effect: The nonlinear distribution of near-bed sediment at fluvial diversions. *Earth Surface Processes and Landforms*, *42*(14), 2322–2337.

Eaton, B. C. (2013). Hydraulic geometry: empirical investigations and theoretical approaches, *Treatise on Geomorphology* (pp. 313–329). San Diego: Academic Press.

Edmonds, D. A. (2012). Stability of backwater-influenced river bifurcations: A study of the Mississippi-Atchafalaya system. *Geophysical Research Letters*, *39*, 8.

Gaweesh, A., & Meselhe, E. (2016). Evaluation of sediment diversion design attributes and their impact on the capture efficiency. *Journal of Hydraulic Engineering*, *142*(5), 4,016,002.

Goodfriend, G. A., & Stanley, D. J. (1999). Rapid strand-plain accretion in the northeastern Nile Delta in the 9th century AD and the demise of the port of Pelusium. *Geology*, *27*(2), 147–150.

Habermaas, F. (1935). Geschiebeeinwanderung in Werkkanäle und deren Verhinderung. *Wasserkraft und Wasserwirtschaft*, *30*(9), 97–116.

Hager, W. H. (1984). An approximate treatment of flow in branches and bends. *Proceedings of the Institution of Mechanical Engineers, Part C: Journal of Mechanical Engineering Science*, *198*(1), 63–69.

Hassenpflug, W. C. (1998). Branched channel free-streamlines. *Computer Methods in Applied Mechanics and Engineering*, *159*(3-4), 329–354.

Herrero, A., Bateman, A., & Medina, V. (2015). Water flow and sediment transport in a 90° channel diversion: An experimental study. *Journal of Hydraulic Research*, *53*(2), 253–263.

Kacimov, A. R. (2000). Note on a paper by Sinha and Odgaard "Application of conformal mapping to diverging open channel flow". *Journal of Engineering Mathematics*, *37*(4), 397–400.

Kalkwijk, J. P. T., & Booij, R. (1986). Adaptation of secondary flow in nearly-horizontal flow. *Journal of Hydraulic Research*, *24*(1), 19–37.

Kästner, K., & Hoitink, A. J. F. (2019). Flow and suspended sediment division at two highly asymmetric bifurcations in a river delta: Implications for channel stability. *Journal of Geophysical Research: Earth Surface*, *124*, 2358–2380. https://doi.org/10.1029/2018JF004994

Kästner, K., Hoitink, A. J. F., Vermeulen, B., Geertsema, T. J., & Ningsih, N. S. (2017). Distributary channels in the fluvial to tidal transition zone. *Journal of Geophysical Research: Earth Surface*, *3*, 696–710. https://doi.org/10.1002/2016JF004075

Kawai, S., Egashra, S., & Ashida, K. (1993). Variation of sediment discharge over the side weir and bed variation in straight open channel. *Doboku Gakkai Ronbunshu*, *1993*(473), 7–15.

Kleinhans, M. G., Ferguson, R. I., Lane, S. N., & Hardy, R. J. (2013). Splitting rivers at their seams: Bifurcations and avulsion. *Earth Surface Processes and Landforms*, *38*(1), 47–61.

Kleinhans, M. G., Jagers, H. R. A., Mosselman, E., & Sloff, C. J. (2008). Bifurcation dynamics and avulsion duration in meandering rivers by one-dimensional and three-dimensional models. *Water Resources Research*, *44*, 8.

Meijer, D. G., & Ksiazek, L. (1994). Sediment distribution in a channel bifurcation, Fluent simulation (*Reports Q1941*). The Netherlands: Delft Hydraulics, Delft.

Mendoza, A., Abad, J. D., Frias, C. E., Ortals, C., Paredes, J., Montoro, H., & Soto-Cortés, G. (2016). Planform dynamics of the Iquitos anabranching structure in the Peruvian Upper Amazon River. *Earth Surface Processes and Landforms*, *41*(7), 961–970.

Modi, P. N., Dandekar, M. M., & Ariel, P. D. (1981). Conformal mapping for channel junction flow. *Journal of the Hydraulics Division*, *107*(12), 1713–1733.

Morozova, G. S. (2005). A review of Holocene avulsions of the Tigris and Euphrates rivers and possible effects on the evolution of civilizations in lower Mesopotamia. *Geoarchaeology*, *20*(4), 401–423.

Neary, V. S., Sotiropoulos, F., & Odgaard, A. J. (1999). Three-dimensional numerical model of lateral-intake inflows. *Journal of Hydraulic Engineering*, *125*(2), 126–140.

Önen, F., & Agaccioglu, H. (2013). Live bed scour at a side-weir intersection located on an alluvial channel. *Irrigation and Drainage*, *62*(4), 488–500.

Ramamurthy, A., Qu, J., & Vo, D. (2007). Numerical and experimental study of dividing open-channel flows. *Journal of Hydraulic Engineering*, *133*(10), 1135–1144.

Raudkivi, A. J. (1993). *Sedimentation: Exclusion and removal of sediment from diverted water, IAHR Design Manual* (Vol. 6). Boca Raton, FL: CRC Press.

Redolfi, M., Zolezzi, G., & Tubino, M. (2016). Free instability of channel bifurcations and morphodynamic influence. *Journal of Fluid Mechanics*, *799*, 476–504.

Riad, K. (1961). *Analytical and experimental study of bed load distribution at alluvial diversions*: TU Delft, Delft University of Technology.

Rozovskii, I. L. (1957). *Flow of water in bends of open channels*. Kiev: Academy of Sciences of the Ukrainian SSR.

Sassi, M. G., Hoitink, A. J. F., Vermeulen, B., & Hidayat, H. (2013). Sediment discharge division at two tidally influenced river bifurcations. *Water Resources Research*, *49*(4), 2119–2134.

Schumm, S. A. (1985). Patterns of alluvial rivers. *Annual Review of Earth and Planetary Sciences*, *13*, 5.

Shettar, A. S., & Murthy, K. K. (1996). A numerical study of division of flow in open channels. *Journal of Hydraulic Research*, *34*(5), 651–675.

Sinha, S. K., & Odgaard, A. J. (1996). Applications of conformal mapping to diverging open channel flows. *Journal of Engineering Mathematics*, *30*(3), 355–363.

Slingerland, R., & Smith, N. D. (1998). Necessary conditions for a meandering-river avulsion. *Geology*, *26*(5), 435–438.

Sloff, K., & Mosselman, E. (2012). Bifurcation modelling in a meandering gravel-sand bed river. *Earth Surface Processes and Landforms*, *37*(14), 1556–1566.

Sloff, K., Van Spijk, A., Stouthamer, E., & Sieben, A. (2013). Understanding and managing the morphology of branches incising into sand-clay deposits in the Dutch Rhine Delta. *International Journal of Sediment Research*, *28*(2), 127–138.

Van der Mark, C. F., & Mosselman, E. (2013). Effects of helical flow in one-dimensional modelling of sediment distribution at river bifurcations. *Earth Surface Processes and Landforms*, *38*(5), 502–511.

Vanoni, V. A. (2006). *Sedimentation engineering*: American Society of Civil Engineers.

Wang, Z. B., De Vries, M., Fokkink, R. J., & Langerak, A. (1995). Stability of river bifurcations in 1D morphodynamic models. *Journal of Hydraulic Research*, *33*(6), 739–750.